THE JOURNAL OF PHYSICAL CHEMISTRY B

ARTICLE

pubs.acs.org/JPCB

Lyotropic Lipid Phases Confined in Cylindrical Pores: Structure and Permeability

Peter Falkman,*[,†] Christoffer Åberg,[†,‡] Anna Clemens,[†,§] and Emma Sparr[†]

[†]Physical Chemistry, Chemical Center, Lund University, P.O. Box 124, SE-221 00 Lund, Sweden

[‡]Centre for BioNano Interactions, School of Chemistry and Chemical Biology, University College Dublin, Belfield, Dublin 4, Ireland

Supporting Information

ABSTRACT: A model membrane system based on lipid lyotropic phases confined inside the pores of a well-defined scaffold membrane, thereby forming a double-porous membrane structure, is described. The model membrane system is characterized with regard to lipid structure, lipid location, and phase transitions, using small-angle X-ray scattering, differential scanning calorimetry, and confocal microscopy. The system enables studies of transport across oriented lipid bilayers as well as of lipids in confinement. The lipids are shown to be located inside the membrane pores, and the effect of confinement on lipid structure is shown to be small, although dependent on the surface properties of the scaffold membrane. For transport studies, Franz diffusion cells and different types of drugs/dyes are used, and the transport studies are complemented with theoretical modeling. Lipids investigated include monoolein, dioleoyl phosphatidylcholine, dimyristoyl phosphatidylcholine, and *E. coli* total lipid extract. In the case of monoolein, the lipid structure can be changed from a bicontinuous cubic *Ia3d* phase to a liquid crystalline lamellar phase, by controlling the osmotic pressure of the surrounding solution through addition of water-soluble polymer. The osmotic pressure can thereby be used as a switch, changing the permeability of the lipid phase up to 100-fold, depending on the properties of the diffusing substance. The large effect of changing the structure implies an alignment of the lamellar phase inside the pores.

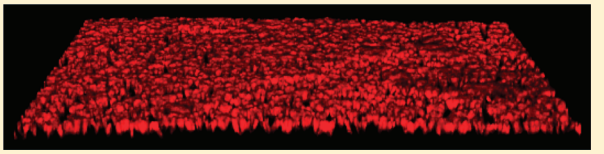

1. INTRODUCTION

The main function of a membrane is to control the exchange of matter between the surrounding regions. In the living system, this membrane typically consists of a single lipid bilayer that separates the different compartments. There are, however, numerous exceptions where several bilayers are stacked, like the extracellular lipids in stratum corneum,[1] the myelin structure around nerve axones,[2] the membranes in retinal rods,[3] the lung surfactant at the alveolar interface,[4] and several examples of stacked bilayers in cell membranes.[5] There are also numerous observations of more complex multilayer arrangements with curved bicontinuous bilayer structures in cell membranes under physiological conditions, for example in the endoplasmic reticulum and the mitochondria, sometimes with interesting connections to pathological conditions.[5−8] Similar membrane structures have been suggested for the lamellar bodies in the stratum granulosum in a lower layer of the skin.[9] All these examples are biological multilayer membranes with complex compositions, and their structure is not static. The exact nature of the self-assembled structure is determined by a delicate balance of intermolecular interactions between membrane molecules and their surroundings, where small changes in the membrane environment can lead to major changes of the self-assembled structure, which in turn can alter the transport properties in the membrane. This possibility of membrane response, in terms of structure and barrier properties, to changes in the surroundings is particularly relevant if the membrane separates environments with profoundly different properties. The mechanism for diffusional transport in responding membranes has previously been described in a theoretical model[10,11] and demonstrated in experimental studies on model lipid membranes.[10,12] It has also been shown that the upper part of the human skin, the stratum corneum, has the properties of a responding membrane in that its barrier properties can be regulated by variations in the outer environment.[13,14] Other practical applications of this mechanism can be found in drug delivery systems composed of particles with lyotropic structures.[7]

The response in the lipid membrane can be predicted on the basis of the equilibrium lipid phase behavior in bulk under different conditions. However, in many situations in biological and technical applications, there can be other complicating aspects of the system that alter the equilibrium structure. One relevant situation is that the lipid lyotropic phase is confined in a smaller volume. Seen as a general phenomenon, confinement of lyotropic phases can, in principle, lead to interfacial interactions, confinement-induced entropy loss, geometrical restrictions that alter swelling, structural frustrations, and capillary-induced changes in the self-assembled structure.[15] It has indeed been established that liquid crystalline materials can be influenced by confinement and the presence of

Received: July 8, 2011
Revised: October 12, 2011
Published: October 18, 2011

nearby surfaces.[15,16] This might be relevant also to the extracellular lipids in the stratum corneum, which form a matrix surrounding dead keratin-filled cells, the corneocytes. As the only continuous route for transport goes through the extracellular lipids, these lipids are considered crucial to the barrier properties of the skin. A notable observation is that the extracellular lipids constitute only a small fraction of the complete stratum corneum (ca. 15%) and that they are confined in between the corneocytes.[1,17] It is not clearly established how the confinement affects the lipid structure and if this is in some way significantly different from the bulk systems composed of extracted stratum corneum lipids or model lipids. It has been suggested that the higher degree of swelling of the corneocytes implies internal stress on the extracellular lipid matrix.[18] Also lyotropic phases in other systems can be affected by confinement. As one example, several experimental and theoretical studies of block copolymer self-assembly in micro- and nanospaces[19−21] show that confinement in nanocylinders or nanocavities can lead to formation of unique mesostructural morphologies.

In the present study, we develop a model membrane system where lyotropic lipid phases are confined inside the pores of a scaffold membrane, which we therefore define as a double-porous membrane. This model membrane system should allow for transport studies through multilayer membrane structures and also enable studies of how confinement affects the membrane properties. We aim at a system with well-defined pore structure, and for this we use so-called track-etch membranes[22] with cylindrical pores with different diameter and different surface treatment. The pores in these scaffold membranes are monodisperse in size and oriented perpendicular to the membrane surface and are filled with lipid lyotropic phases. Here, we study double-porous model membranes formed from different lipid systems, including monoolein (MO), dioleoyl phosphatidyl choline (DOPC), dimyristoyl phosphatidyl choline (DMPC), and *Escherichia coli* lipid extract. Depending on the lipid system and external conditions in osmotic pressure (Π_{osm}) and temperature, different lipid structures such as the gel lamellar phase, liquid crystalline lamellar phase, and bicontinuous cubic (*Pn*3*m* and *Ia*3*d*) phases are formed inside the pores. By using a combination of experimental techniques, including confocal fluorescence microscopy, small-angle X-ray scattering (SAXS), differential scanning calorimetry (DSC), and diffusion cell systems, we are able to characterize these systems in terms of lipid location, lipid phase structure, and phase transitions of the confined lyotropic phases.

For the transport studies, it is essential that the model membrane is well aligned and that it is more or less free of local defects, as this clearly has a strong influence on the transport properties. Our transport data imply that the present setup using well-defined scaffold membranes with cylindrical pores is superior in preventing defects and in inducing orientation of anisotropic phases, compared to lipid lyotropic phases deposited on top of supporting membranes[12,23] or inside meshlike porous membranes.[10] We finally explore this model system for studies of diffusional transport of drug/dye molecules in the presence of an external osmotic gradient that alters phase structure inside the membrane, demonstrating the properties of a responding lipid membrane. We furthermore note that the present approach of confining the lyotropic phase inside monodisperse pores also provides a way to study phase behavior in confined spaces, as an alternative to X-ray surface force apparatus.[24] The use of scaffold membranes with different surface treatment further enables us to tune the interfacial interactions. If the double-porous model membrane system is equilibrated with bulk solutions with given

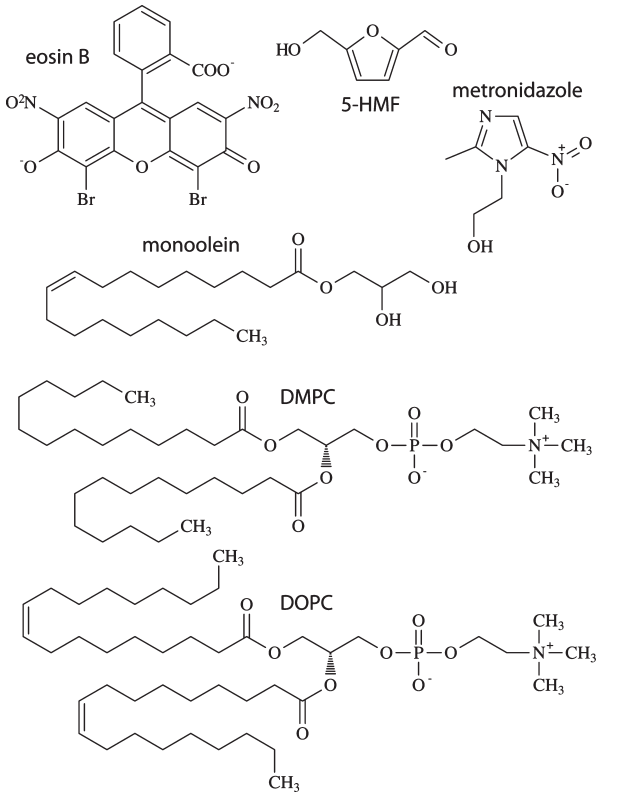

Figure 1. Chemical structures of the drugs/dyes and lipids used.

properties, for example, physiological water chemical potential (i.e., Π_{osm} corresponding to physiological salt solution), it is also possible to study macromolecules in confined spaces and still maintain relevant physiological water chemical potential in the system. This condition is indeed often violated in so-called crowding experiments where water-soluble polymers like PEG are used as crowding agents but also concomitantly alter the water chemical potential to values that are different from the physiological water chemical potential.

The model membrane system presented here represents an alternative to other types of stabilized bilayers, such as tethered lipid bilayers,[25] black lipid membranes,[26] nanoblack lipid membranes,[27] and other bilayer films.[28] There are also examples of model membrane systems where lipids are confined inside pores in anodized aluminum oxide (AAO) membranes where they form concentrical cylinders.[29] The AAO scaffold membrane differs from the present track-etch membranes used here both in terms of surface properties and in that the pore diameter is not constant throughout the entire membrane. The same type of AAO membranes, as well as anodized silicone membranes, has been used to study another system, the nematic to smectic phase transition of 4-*n*-octyl-4′-cyanobiphenyl, where large effects on the phase behavior have been detected.[30]

2. EXPERIMENTAL METHODS

2.1. Materials. 1,2-Dimyristoyl-sn-glycero-3-phosphocholine (DMPC) was purchased from Larodan (Sweden). 1,2-Dioleoyl-sn-glycero-3-phosphocholine (DOPC) and *E. coli* total lipid extract (57% phosphatidylethanolamine, 15% phosphatidylglycerol, 10% cardiolipin) were purchased from Avanti Polar Lipids (USA). Eosin B (Certistain) and cyclohexane (p.a.) were purchased from

Merck Chemicals (Germany). 2-methyl-5-nitro-1-imidazoleethanol (metronidazole) (≥98%, Fluka), polyethylene glycol M_W 2000 (PEG 2000) (Fluka), and 5-(hydroxymethyl)-furfural (5-HMF) (≥99%, Aldrich) were purchased from Sigma-Aldrich (USA). Ethanol 99.5% was purchased from Kemetyl (Sweden). Structural formulas for dyes/drugs and lipids used can be found in Figure 1.

MO was a kind gift from Axel Borerup, Danisco Ingredients (Denmark). The MO (batch 173403) is of technical grade and consists of ca. 95% monoglycerides, the rest being mainly diglycerides, fatty acids, and free glycerol. The MO content is ca. 90%. The phase behavior of this and comparable commercial samples from the same source is well characterized, and it is similar to that of pure MO, although the exact positions of the phase boundaries are slightly shifted.[31−33] The bulk phase behavior of the batch was previously checked by letting samples of hydrated MO (around 30 wt %) equilibrate inside a dialysis membrane (Spectra/Por, lot 09593, cutoff 1000) with aqueous solutions of PEG 8000 of different concentrations.[10]

Alexa Fluor 680-labeled dextran M_W 3000 and lipid analogue Lissamine (rhodamine B-labeled DHPE) were purchased from Invitrogen (USA).

Track-etch polycarbonate membranes (∅ 25 mm), both hydrophobic (uncoated) and hydrophilic (PVP-coated), with pore diameter 0.1 and 1.0 μm were purchased from Sterlitech (USA). Cellulose ester dialysis membranes, Spectra/Por lot 3233427, molecular weight cutoff 100 000 and 1000 were purchased from Spectrum Laboratories (USA). All solutions were prepared using high-quality Milli-Q water (Millipore).

2.2. Preparation of Lipid-Filled Membranes. Polymer scaffold membranes were weighed, carefully dipped into a solution of lipid in ethanol, and allowed to dry. Residual ethanol was evaporated under vacuum for at least 4 h, after which the lipid-filled membranes were weighed again to determine total lipid content. Membranes were handled with care and only touched, using tweezers, in the outer part (which was not exposed in the transport experiments, as the diffusion area of the Franz cell is smaller than the membrane diameter). For membranes with pore diameter 0.1 μm, a solution with 0.050 g/mL of lipid was used, and for membranes with pore diameter 1.0 μm, either 0.100 or 0.075 g/mL of lipid was used (higher lipid content is needed to fill the larger pores, as the total pore volume is larger). For *E. coli* total lipid extract, 0.050 g/mL of lipid in ethanol/cyclohexane 1/1 was used, as ethanol in itself could not completely dissolve the lipids.

2.3. Confocal Laser Scanning Microscopy. The confocal laser scanning microscopy was performed on a Fujitsu Siemens LSM510 META (Zeiss). Polymer scaffold membranes were dipped in lipid solution of the same concentration as described above, using a lipid solution containing addition of lipid analogue Lissamine (rhodamine B-labeled DHPE) at a ratio of 10^{-3}/1 to the lipid content. The lipid-filled membranes were carefully hydrated in either water or aqueous solution containing Alexa Fluor 680-labeled dextran (10 μg/mL) and mounted on microscopy slides. Stacks of confocal images, from different heights in the sample (Z-stacks), were obtained to allow the construction of 3D representations of the lipid-filled membranes. Corresponding experiments were also performed on empty polymer scaffold membranes, with only aqueous solution containing Alexa Fluor 680-labeled dextran.

2.4. Small-Angle X-ray Scattering. Lipid-filled membranes were cut into pieces of suitable size, placed in either water or aqueous PEG solution, allowed to equilibrate, and finally stacked (∼15 membrane slices per sample) between mica sheets in a vacuum-sealed solid sample holder. Additional water or PEG aqueous solution was added to fill up the sample holder. Bulk lipid samples were handled and hydrated in a corresponding way. As it was not possible to achieve perfect alignment of the small membrane pieces in the sample holder, we were not able to study the bilayer orientation within the pores in the SAXS experiments. Samples were examined using SAXS with a synchrotron X-ray source at beamline I711 at MAX-Lab (Lund University).[34,35] The radiation wavelength was 1.1 Å, and diffractograms were recorded at room temperature (25 °C) using a MAR CCD 165 2D detector. The exposure time was 600 s for each membrane sample and 60 s for each bulk sample. The resulting CCD images were integrated using the Fit2D software provided by Dr. A. Hammersley (http://www.esrf.eu/computing/scientific/FIT2D/).

Table 1. Correspondence between Osmotic Pressure, Relative Humidity, and wt % PEG 2000 for the Solutions Used[36,37]

Π_{osm} (MPa)	RH (%)	wt % PEG 2000
0.69	99.5	18.7
1.38	99	25.9
2.78	98	33.8
3.48	97.5	36.5
4.19	97	38.8
6.33	95.5	44.0
8.51	94	47.9
12.97	91	53.6
20.70	86	60.2

2.5. Differential Scanning Calorimetry. Lipid-filled membranes were cut into pieces of suitable size and stacked in coated aluminum pans (TA Instruments, New Castle, DE, ref no. 900790.901 and 900796.901). A total of 1 mg of lipid-filled membrane, corresponding to 0.1 mg or 0.05 mg of lipid for 1.0 and 0.1 μm pore diameter membranes, was put into each pan. For the pure lipid samples, 2 mg of lipid was used. The samples were hydrated with 10 mg of water and the pans hermetically sealed. Samples were analyzed using a DSC 6200 calorimeter (Seiko Instruments, Inc., Shizouka, Japan), at a heating rate of 5 °C/min. An empty sample pan was used as reference. Both the heating and the cooling cycles were monitored, although only the heating cycle results were used in the final analysis. Two samples of each type (different membrane types and pore diameters) were analyzed, and each sample was run several times to ensure reproducibility. Transition temperature was determined as mean ± standard error of the mean (SEM) of the maximum/minimum of the peak, T_m, for each type.

2.6. Transport Experiment Setup. A lipid-filled membrane was placed between two dialysis membranes (cutoff 100 000 Da), in a Franz diffusion cell with receptor chamber volume of 5 mL, donor chamber volume of 1 mL, and diffusion area of 0.636 cm^2. Π_{osm} on either side of the membrane was controlled by the addition of water-soluble polymer (PEG 2000) and set to Π_{osm} = 0.69 MPa in the receptor chamber solution and Π_{osm} = 0.69−20.70 MPa in the donor chamber solution. For the relation between PEG concentration and Π_{osm}, see Table 1.[36,37] The Franz cell was left to reach steady state overnight at 25 °C. The boundary conditions are given by Π_{osm} in the surrounding solutions, and these determine the gradient in water chemical potential across the lipid in the membrane.[38]

At the start of the experiment, the solution in the donor chamber was exchanged for 900 μL of solution with the same PEG content

but with an addition of the dye/drug to be investigated (1 mg/mL for eosin B and metronidazole, 0.25 mg/mL for 5-HMF). The solution in the receptor chamber was stirred using an IKA RO 5 P magnetic stirrer and recirculated via an Ismatec peristaltic pump to a flow-through quartz cuvette, inside a Cary 300 Bio UV−visible spectrophotometer. The absorbance at the maximum absorbance wavelength (518 nm for eosin B, 319 nm for metronidazole, 284 nm for 5-HMF) was measured in four Franz cells in parallel, once a minute for at least 12 h. The concentration in the donor chamber was chosen such that the concentration in the receptor solution during the experiment was high enough to give an absorbance within the detectable range and also such that the change in concentration in the donor chamber during the experiment was negligible. If the boundary conditions in the donor and receptor solutions remain constant over the period of the experiment, the system eventually reaches steady state in terms of both the osmotic gradient and the gradient in drug/dye investigated. The constant steady-state flux is characterized by a linear increase in concentration on the receptor side, as shown in Figure 2 (upper curve). Since the concentrations in donor and receptor chamber are not completely unaltered throughout the entire 12 h experiment, due to the diffusional transport of model substance and water across the membrane, we only use data from the initial part of the linear regime to calculate the flux (as indicated in Figure 2).

From the total volume of the receptor chamber, the tubing, and the cuvette (V), the slope of the concentration change over time ($c'(t)$) could be recalculated to an amount transported over time. Corrected for available diffusion area (A), which is the total available cross-sectional pore area exposed inside the Franz cell (available membrane area × pore density × single pore area), this gives the flux across the lipid lyotropic phase. The effective permeability (P_{eff}) is then obtained as

$$P_{eff} = \frac{\text{Flux}}{\Delta C} = \frac{c'(t) \times V}{A \times \Delta C} \quad (1)$$

where ΔC is the gradient in drug/dye concentration.

P_{eff} was measured several times (3−10) for each lipid system and Π_{osm}, and the mean and standard error of the mean (SEM) were calculated for each set of conditions.

2.7. MO/Water Partition. The partition coefficient of the different dyes/drugs between MO and water was determined. This was done by making a stock solution of eosin B/metronidazole/5-HMF, mixing 2 g of it with 0.1 g of MO, and equilibrating for at least 2 weeks. After the sample was centrifuged for at least 12 h, the absorbance of the water phase, as well as of the remaining stock solution, was measured. Here, the concentration of the stock solution was chosen so that the absorbance of both the sample and the stock solution could be measured without dilution. Log $P_{MO/W}$ was calculated from the measured weights of MO and stock solutions, the densities of water and MO, and the absorbances measured. All determinations were done in triplicate.

2.8. Phase Characterization of Bulk Samples. To assess the effect of 5-HMF on MO structure without the risk of PEG incorporation into the lipid phase, MO was placed inside a semipermeable membrane (cutoff 1000 Da) and exposed to a PEG solution also containing 5-HMF ($\Pi_{osm} > \Pi_{tr}$ for pure MO). After equilibration, the lipid was inspected both visually between crossed polarizers and with regard to viscosity. This allows easy distinction between a cubic phase (isotropic, stiff) and a lamellar one (anisotropic, less viscous).

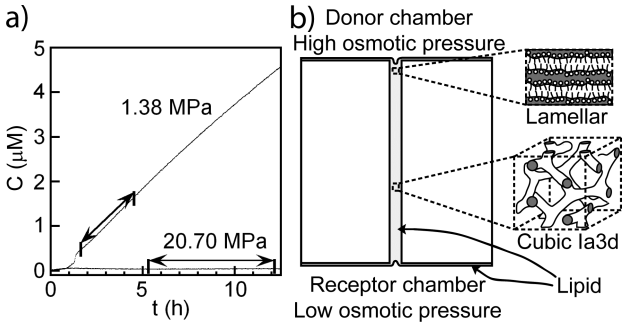

Figure 2. (a) Raw data from the MO transport experiment, with eosin B concentration in the cuvette as a function of time, for high and low osmotic pressure in the donor chamber. The arrows indicate the first, linear part, used for calculations. (b) Schematic representation of the lipid phase inside the membrane pores, with high osmotic pressure at one side of the membrane. Corresponds to the lower line (20.70 MPa) in the left-hand graph.

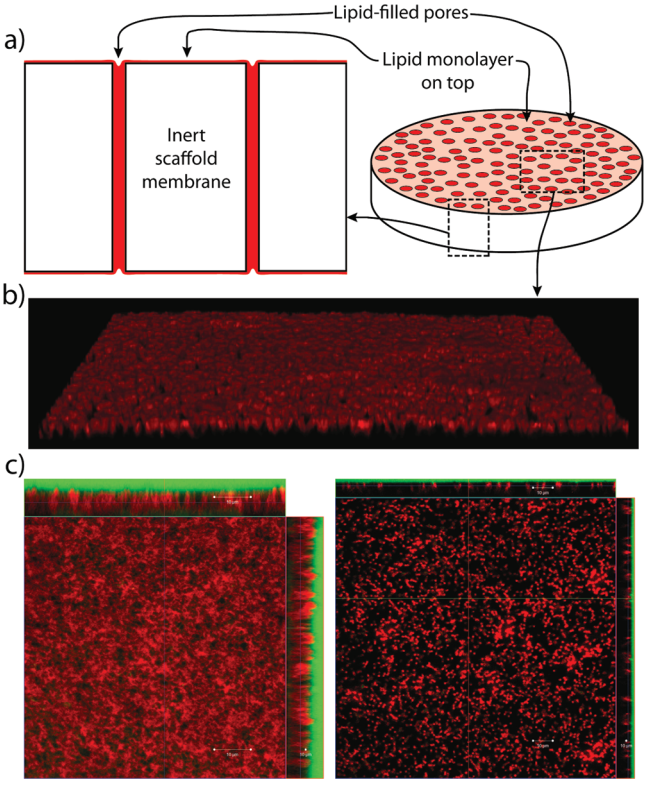

Figure 3. (a) Schematic illustration of a lipid-filled porous membrane (right), with cut out view from the side (left), (b) confocal 3D representation of a section of the membrane, and (c) confocal images with orthogonal view representations in the side panels of 0.1 μm pores (left) and 1.0 μm pores (right). Lipid in red; labeled dextran in green (lower images). Schematic images (a) are not drawn to scale. Note the different scales in panel c.

3. RESULTS AND DISCUSSION

3.1. Double-Porous Membrane. We aim at a double-porous membrane, where lyotropic phases confined inside the well-defined pores of an inert scaffold membrane form a double-porous structure. Figure 3a shows a schematic illustration of such a model membrane system. The preparation requires both homogeneous distribution of

the lipid material inside the pores and that molecularly ordered lyotropic phases form inside the pores upon hydration. The protocol developed to accomplish this includes dissolving the lipid in organic solvent, dipping the polymer scaffold membrane in this solution, and then allowing it to dry. We chose to use hydrophobic polycarbonate track-etch membranes with cylindrical pores that are monodisperse in size and arranged perpendicular to the polymer membrane surface. Since many organic solvents that dissolve the lipids (e.g., chloroform) also dissolve the polycarbonate membrane, the choice of solvent was not straightforward, and ethanol was finally chosen as the best solvent to use. Care had to be taken to ensure that the lipid deposited inside the pores and not only on the polymer membrane surface. This is obviously related to the surface properties of the polymer scaffold membrane, the solvent used, the evaporation rate, and the preparation procedure.[10,12] The procedure of carefully turning the polymer scaffold membrane while it dries appears to be the best method of preparation, as this prevents the evaporating solution from gathering at either side. As more and more solvent evaporates, the remaining solution is pulled into the pores by surface tension, and the lipid precipitates there. A thin layer of lipid will likely also deposit on the outer surface of the membrane, possibly forming a monolayer at the hydrophobic surface, but the majority of the lipid should be confined inside the membrane pores. Polymer scaffold membranes with different pore diameters (1.0 and 0.1 μm) and different surface properties (untreated type with hydrophobic surface and a PVP-treated type with more hydrophilic surface) were used. The thickness of these polymer scaffold membranes is either 11 or 6 μm, respectively, for the different pore diameters. Deposition of lipids inside the pores was accomplished for all pore diameters and polymer membrane types, and double-porous membranes were formed from several types of lipids including MO, DOPC, DMPC, and *E. coli* total lipid extract. Weighing of membranes before and after dipping showed slight differences in deposited amounts for different lipids, which was easily remedied by adjusting the lipid concentration of the dipping solution.

3.2. Lipid Confinement. It is crucial to verify that the lipid phase is actually confined inside the pores and not deposited on top of the scaffold membrane. The lipid distribution inside the polymer scaffold membrane was visualized with confocal microscopy by including a small amount (0.1 mol %) of a fluorescent lipid analogue (red) in the lipid phase and fluorescently labeled dextran (green) added to the water phase. By taking several images of the sample at different depths, a 3D model could be constructed. Figure 3b shows a rendering of this 3D stack with a view slightly from above, showing pores with diameter 1.0 μm filled with lipid (red). In Figure 3c, one confocal plane of such a 3D model is shown, together with orthogonal representations of the side views in the side panels. Here, images for track-etch membranes with pore diameters of 1 and 0.1 μm are shown. As the size of the 0.1 μm pores is below the resolution limit, individual pores cannot be distinguished. However, it is clear from the images that the lipid is confined inside the pores and not present on the exterior surface to any significant extent. It is also clear that the water-soluble polymer (green) does not penetrate into the polymer scaffold membrane, ruling out empty, unfilled pores. This observation also allows us to exclude the possibility that lipids only cover the pore walls as a thin film. For the larger pore diameters (1.0 μm, lower right), partially unfilled pores are sometimes visualized at lower lipid contents, showing cases where the lipids only cover the pore walls but not the center of the pores. For these cases, we also observe penetration of the water-soluble polymer into the outer parts of the pore close to the membrane surface. However, no completely unfilled pores were found. Confocal microscopy on empty polymer scaffold membranes (without lipid), in an aqueous solution with fluorescently labeled dextran, showed both water penetration into the pores and water phase outside the polymer scaffold membrane (not shown). We also note that by varying the amount of lipid in the lipid-filled membranes, which is achieved by varying the lipid concentration in the solvent during preparation, it is possible to tune the number of unfilled pores.

The lipid distribution inside the pores did not show any difference between the different lipid systems investigated. An optimal range of lipid content for the different polymer membrane types could thus be determined, where the balance between having no unfilled pores and no lipid layer deposited on the exterior surface of the support membranes was deemed the most beneficial. Only lipid-filled membranes falling within this range were used in the study. The risk of unfilled or partially unfilled pores was deemed higher for the larger pore diameter, and therefore the polymer scaffold membranes with the smaller pore diameter, 0.1 μm, were chosen for the transport studies.

3.3. Lipid Phase Behavior in Confinement. In the double-porous membranes, the lipid lyotropic phases are confined inside small cylindrical pores. This implies a large contact area between the lipid phase and the polycarbonate scaffold, and potentially this interaction can affect lipid phase structure and phase transitions.[15,39] To investigate the phase behavior of lipids confined inside the scaffold membrane, small-angle X-ray scattering (SAXS) studies were performed on double-porous membranes filled with different lipid lyotropic phases and at different Π_{osm}. The results were then compared to bulk lipid phase behavior[33] and, for the case of MO, also to phase behavior inside tortuous pore PVF membranes.[10] A major obstacle in these experiments is the low signal due to small amount of lipid in the sample, as the pores only constitute a minor fraction of the scaffold membrane. Therefore, we were only able to obtain well-resolved data for the double-porous lipid membranes with a diameter of 1.0 μm, while for the membranes with smaller size pores the intensity from the lipids was too low. Even for the larger pore diameter, the total amount of lipid possible to get into a sample was as low as 30 μg, and only synchrotron SAXS was sensitive enough to clearly reveal the Bragg reflections.

Figure 4 shows the scattering intensity as a function of the magnitude of the scattering vector, q, for double-porous track-etch membranes filled with different types of lipid lyotropic phases. The membrane pieces were hydrated in aqueous solution with known Π_{osm}, as controlled by adding different amounts of the polymer polyethylene glycol (PEG) to the surrounding solution.[38,40] The diffraction pattern for the double-porous MO membrane hydrated with PEG solution at Π_{osm} = 0.69 MPa is shown in Figure 4a. Eight peaks are indicated in the figure, which are all consistent with a cubic *Ia*3*d* structure with a unit cell size of 123 Å. This value is close to the unit cell size of 121 Å obtained from bulk measurement of the technical grade MO from the same batch under the same Π_{osm} and to previously reported data for technical grade MO in tortuous pore membranes (Π_{osm} = 0.66 MPa)[10] which showed a unit cell dimension of 120 Å. We also note that these values are all slightly lower compared to previous reports in the literature, where the bulk MO *Ia*3*d* cubic phase unit cell size at Π_{osm} = 0.69 MPa was measured to be 130 Å.[40] The difference can

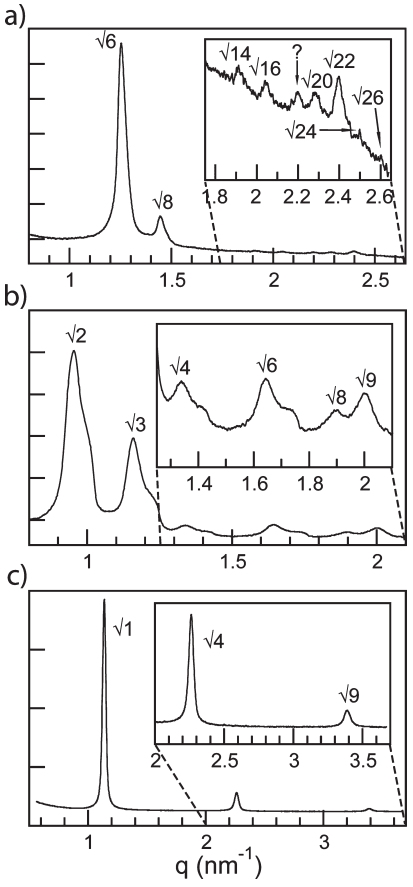

Figure 4. SAXS data for lipid-filled membrane, pore diameter 1.0 um, in (a) MO in PEG solution (Π_{osm} = 0.69 MPa), (b) MO in pure water, and (c) DOPC in PEG solution (Π_{osm} = 0.69 MPa). Insets show magnifications of part of the *q*-range. In (a), the question mark indicates one peak unaccounted for.

most likely be explained by the MO samples coming from different batches with different purities.

In the diffraction pattern in Figure 4a, there is also an additional peak at 2.20 nm^{-1}, as indicated by a question mark. The position of this peak is almost exactly between $\sqrt{18}$ and $\sqrt{19}$, and at present we have no explanation for this. A weak peak at the same relative position was also observed in previous data for MO in tortuous scaffold membranes.[10] From the reference experiments on the empty polymer scaffold membrane in PEG solution (Π_{osm} = 0.69 MPa), we concluded that the peak is not likely to originate from the scaffold membrane itself. The diffraction pattern for the empty scaffold membrane showed four very minor peaks, at 1.32, 1.50, 1.99, and 2.87 nm^{-1}, all of them too weak to be distinguishable in the presence of a reflecting sample. There was no peak observed at 2.20 nm^{-1}.

Figure 4b shows the scattering data for the same type of MO-filled membranes equilibrated in pure water (Π_{osm} = 0). Six peaks are indicated and consistent with a cubic *Pn*3*m* structure with a unit cell size of 93 Å. This is consistent with our measurement of the bulk MO phase under the same conditions and from the same batch, which show the same phase with a unit cell size of 92 Å. Again, the unit cell size is slightly lower compared to literature data for bulk samples, reported at 101 Å.[40]

At high Π_{osm}, the MO system forms a lamellar phase,[10,12,41] which was also confirmed for bulk samples in the present system. At Π_{osm} = 20.70 MPa, the lamellar phase repeat distance was measured to be 62 Å. This value is higher compared to previously reported data for the repeat distance in the MO lamellar phase.[10,33] A practical complication in the present experiments is that, due to the limited size of the SAXS sample holder, it was not possible to prepare the samples with a semipermeable membrane separating the lipid and the PEG solution. Even though one generally can assume segregative phase separation between the lipid phase and the aqueous PEG solution, this is not necessarily applicable to the MO−PEG−water system. It has indeed been shown that even high molecular weight PEG can be incorporated in bicontinuous cubic phases and thus alter the dimensions of the phases as well as the position of the phase boundary,[42] which might explain the observed discrepancies between the observed values and literature data. As will be described later, precautions were taken in the transport studies where a semipermeable membrane separates the PEG solution and the double-porous lipid membranes.

The phase behavior of other lipid systems inside the pores of the scaffold track-etch membrane was also investigated. Figure 4c shows the diffraction pattern for DOPC in PEG solution (Π_{osm} = 0.69 MPa). Three equidistant peaks are detected, indicating a lamellar structure with repeat distance of 55 Å, and the same value was obtained for the bulk phase DOPC sample under the same conditions. This also agrees with literature data for DOPC.[43] Bulk samples of *E. coli* total lipid extract were also investigated, showing several rather smeared out peaks that seem to indicate coexistence between two or more phases, of which one is a highly swollen lamellar phase. *E. coli* total lipid extract in TRIS buffer with NaCl has previously been shown to exhibit hexagonal packing at room temperature and *Pn*3*m* and *Im*3*m* cubic packing at elevated temperatures.[44] *E. coli* lipids from a different source were shown to have lamellar packing close to the bacterial growth temperature and hexagonal or cubic packing at higher temperatures.[45]

To summarize this section, we conclude that all the lipid systems investigated form lyotropic phases inside the pores when hydrated. Furthermore, we conclude that the confinement of lipids inside cylindrical pores with diameter 1.0 μm has no detectable effect on the lipid phase behavior or the unit cell sizes as compared to the bulk phase samples. Still, we cannot exclude such effects in smaller sized pores.

3.4. Transport through Oriented Double-Porous Lipid Membranes. One major motivation for the development of the double-porous membrane is to enable studies of diffusional transport across multilayer lipid membranes. Diffusional transport of any substance that does not partition equally between a lipid and an aqueous phase is very sensitive to the lipid phase behavior and the orientation of anisotropic phases inside the pores. Therefore, we aim to control not only confinement and phase behavior but also the orientation of anisotropic lyotropic phases inside the pores. For a lamellar phase, we can envision either that the bilayers are oriented with the bilayer normal parallel to the pore walls or that they form concentric cylinders inside the pores. A priori we cannot predict which one is preferred, but by the preparation procedure described we hope to avoid a completely random orientation.

The orientation of an anisotropic phase inside the pores likely depends on the system and the preparation procedure. The literature shows that single bilayer black lipid films on the surface of porous AAO membranes, with the outer membrane surface covered with a hydrophobic functionalized gold layer, are

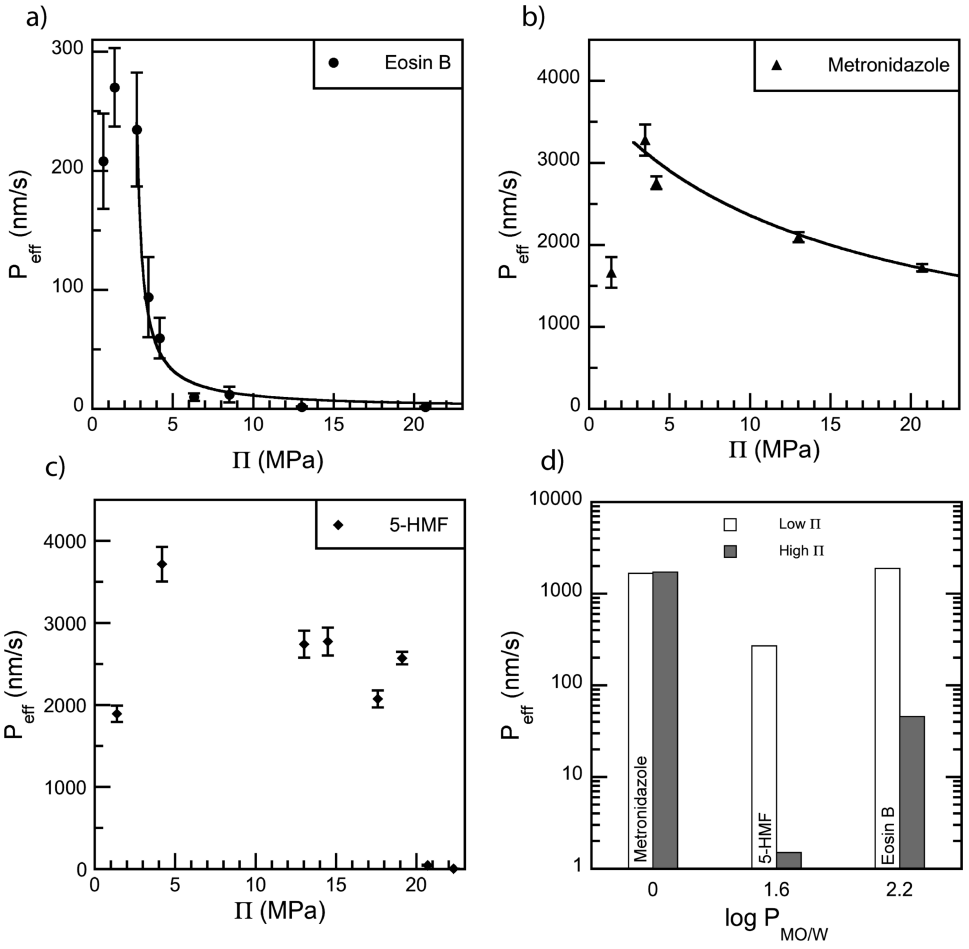

Figure 5. Effective permeability (mean ± SEM) across membranes filled with MO, at different osmotic pressures for (a) eosin B, (b) metronidazole, and (c) 5-HMF. The solid lines in panels a,b show the decay of the permeability after the induction of the lamellar phase according to the thermodynamical model,[10,12] with parameters adjusted to agree with the experimental data. In (d), P_{eff} at low (1.38 MPa) and high osmotic pressure (20.70 MPa) is summarized for the three different substances. Note the logarithmic scale of the *y*-axis.

oriented with the bilayer normal parallel to the walls of the support.[46] Similar alignment, with the bilayer normal parallel to the pore walls, was seen for single bilayer lipid films deposited in the pores of polycarbonate membranes,[28] which have surface properties similar to our system. Neutron diffraction experiments on lipids in confined sample geometry (1 mm gap) have further shown that upon confinement bicelle disks transform into orientationally aligned domains of the lamellar phase with very few defects.[47] On the other hand, studies of vesicle-deposited bilayers inside hydrophilic AAO membranes with cylindrical pores (diameter 0.1−0.2 μm) have demonstrated 1−4 concentric bilayers inside the pores.[29] In the latter case, the membrane surface is relatively hydrophilic, and the amount of deposited lipid is low, only allowing coverage of the pore walls and not filling of the entire pore. Indeed, the confocal microscopy studies performed in this work also suggests a similar picture for the present model membrane system under the conditions where there is only a limited amount of lipid present.

Diffusional transport through an anisotropic phase is strongly affected by its orientation, and for most substances it is significantly slower in the direction perpendicular to the bilayer plane, compared to the direction parallel to the bilayer planes. It is therefore possible to use the transport measurements as an indicator for bilayer alignment, orientation, and integrity. To check whether it is possible to obtain an oriented bilayer system with few defects in the double-porous track-etch lipid membranes, we performed studies on diffusional transport of model substances across membranes composed of lipids that form an anisotropic lamellar phase and isotropic bicontinuous cubic phase (see Figure 2). The results obtained for the track-etch scaffold membranes were then compared to previous studies of the same system using different model membrane setups, with either less well-defined mesh-like scaffold membranes or with a lipid lyotropic phase deposited on top of a support membrane.[10,12]

Figure 5a shows the eosin B permeability for transport across a MO membrane as a function of external osmotic gradient. These results were obtained with a constant gradient in eosin B but varying the external osmotic gradient to modulate the phase behavior inside the double-porous membrane, as described in detail in section 2.6. We observe a dramatic decrease in permeability when Π_{osm} in the donor chamber exceeds roughly 3 MPa and a further decay with increasing osmotic gradient. The results can be understood on the basis of the MO phase behavior in bulk[33,40] and inside the pores of the scaffold membranes as follows: For low osmotic gradients, the whole MO membrane is in a bicontinuous cubic phase,[33] where the bilayers extend homogeneously in three dimensions and are continuous with respect to both lipid and water. Therefore, diffusion of both polar and apolar substances is

dx.doi.org/10.1021/jp206451c |*J. Phys. Chem. B* 2011, 115, 14450–14461

typically rapid in all directions. As Π_{osm} in the donor chamber exceeds the cubic to lamellar phase transition, the part of the MO membrane closest to the donor solution forms a lamellar phase (Figure 2b). If the lamellar phase is oriented with the bilayer normal parallel to the direction of transport, we expect both polar and apolar species to experience a reduced permeability. Indeed, the Π_{osm} for which the dramatic decrease in permeability occurs agrees with the bicontinuous cubic to lamellar phase transition in bulk ($\Pi_{osm} \approx 3$ MPa[10,12,41] at 25 °C). As the osmotic gradient is increased even further, more lamellae are formed with a corresponding decreased permeability. This discussion can be made quantitative based on the previously published model,[10] as described in section 3.6 below.

The magnitude of the reduction in permeability (100-fold) with increasing osmotic gradient holds information about the orientation and integrity of the lamellar phase. This large reduction most likely indicates a well-aligned lamellar phase with the bilayer normal parallel to the pore walls and relatively defect-free lamellae. Indeed, the data in Figure 5a should be compared to previous studies of eosin B flux over MO membranes at varying osmotic gradients, obtained for different model systems using different polymer scaffold or support membranes. In these studies, the lipids were spread either on top of a hydrophilic support membrane[12] or inside a meshlike hydrophobic scaffold membrane.[10] In both these systems, it was possible to demonstrate that the transition between a bicontinuous cubic phase and lamellar phase in parts of the responding lipid membrane can regulate the membrane permeability with a switch-like response. However, the reduction of permeability due to the phase transition was smaller than expected (only 2−4 times lower) and clearly much smaller than in the present study. We also note that when lipids were confined inside the pores of the track-etch membranes with larger pores (diameter 1.0 μm) the reduction of permeability due to the phase transition was also smaller than expected (ca. 2 times), and the experimental error was relatively large. One possible explanation for this is that the bilayers in these other model membrane systems did not exhibit as high a degree of orientation as the present model system with small size pores. Another contribution to the difference probably lies in that it is very difficult to produce defect-free bilayer systems. The presence of defects strongly affects the transport properties as these provide other routes for diffusion. With the procedure described here, we believe that the polymer scaffold in the track-etch membranes with small pore size (diameter 0.1 μm) provides a mechanical robustness that to a large extent prevents defects in the lyotropic phases.

3.5. Transport of Model Substances with Different Properties. Figure 5 illustrates how changes in lipid phase behavior affect membrane permeability for substances with different solubilities in the aqueous and the lipid layers. For substances that strongly partition in either the lipid or the water phase, the formation of the lamellar phase will substantially hinder diffusional transport in the direction normal to the orientation of the lamellar plane. This can be understood in terms of a simple solubility−diffusion model, where one assumes that the transport of substance i through the lipid and aqueous regions can be characterized by a single diffusion coefficient, D_i^L and D_i^W, respectively, and that the local concentration in the bilayer can be related to the lipid/bilayer partition coefficient, K_i. Within this framework one can show that at steady state the permeability, P_i, in the direction of the lamellae normals of an oriented lamellar phase is given by[48]

$$\frac{1}{P_i} = \frac{L}{K_i D_i^L} + \frac{W}{D_i^W} \quad (2)$$

Here, the total thickness of the lipid bilayers is given by L, while W is the total thickness of the interlamellar aqueous layers. Since the local mobility within the fluid apolar part of the bilayer is not significantly different from that in bulk water, the diffusion coefficients D_i^L and D_i^W can be considered roughly equal.[49] From eq 2, we see that the permeability of the lamellar phase strongly depends on the partition coefficient K_i. In contrast, we do not expect such strong dependence on K_i when considering transport through a bicontinuous cubic phase, as this structure offers continuous paths through both the aqueous and the lipid regions. The same argument would apply to a lamellar phase with concentric alignment. One may discuss the validity of the solubility diffusion model,[50] but regardless the conclusion that the permeability of a lamellar phase is strongly dependent on its orientation is undoubtedly true.

We have studied diffusional transport of different dyes or drugs across the responding MO membrane at varying osmotic gradient with the same approach as described above. The compounds chosen are eosin B, metronidazole, and 5-HMF. As shown in Table 2 and Figure 1, eosin B is fairly large, highly soluble in water, and charged; metronidazole is small, net uncharged, and slightly soluble in water at most pH values; and 5-HMF is small, uncharged at the relevant pH, and soluble in water. To assess how these different drugs/dyes partition to the lipid phase, we first look at the partition coefficient between octanol and water, $P_{O/W}$, which can be obtained from literature data.[12,51,52] $P_{O/W}$ gives a fair estimate also for the partitioning between liquid crystalline lipid bilayers and water for substances that are hydrophilic or hydrophobic. However, this measure does decidedly worse at predicting the lipid bilayer partitioning for substances of an amphiphilic nature, which indeed applies to most water-soluble dyes. Amphiphilic compounds preferentially locate at the interface between oil and water, which for an octanol bulk sample is quite small (the cross-sectional area of the container), while it is huge for, for example, a bicontinuous cubic phase (500−600 m^2/g MO[53]) or a lamellar phase. Since the present measurements are performed for lipid membranes in the water phase, this means that the partitioning of the investigated substances into the lipid phase may be severely underestimated by using only $P_{O/W}$ data. We therefore determined the partition between the MO bicontinuous cubic phase and water, $P_{MO/W}$, for all substances used. The results for $P_{MO/W}$ and the literature values for $P_{O/W}$ are given in Table 2. As expected, $P_{O/W}$ for metronidazole, which partitions equally between octanol and water, corresponds rather well with $P_{MO/W}$. Eosin B, on the other hand, has a low solubility in octanol,

Table 2. Literature and Experimental Data for the Model Substances Used[a]

substance	eosin B	metronidazole	5-HMF
log $P_{O/W}$	−2.2[12]	−0.3−0.02[51,52]	−0.45[71]
log $P_{MO/W}$	1.59 ± 0.08	−0.01 ± 0.05	2.15 ± 0.31
M_W	580.1	171.2	126.1
pK_a	-	2.6[71]	12.8[71]
sol	300[72]	7[71]	48[71]

[a] log partition octanol/water, measured log partition MO/water (mean ± std deviation), molecular weight, pK_a, and water solubility (g/L).

and is rather amphiphilic, and therefore has a low $P_{O/W}$ but a high $P_{MO/W}$. 5-HMF has slightly higher solubility in octanol compared to water than eosin B, but it is also more amphiphilic, thus giving a low $P_{O/W}$ and a high $P_{MO/W}$.

In relating these data to the transport studies, we take both values $P_{MO/W}$ and $P_{O/W}$ into account. The partitioning into the lipid membrane is determined by the $P_{MO/W}$ partition coefficient, while the process of traversing the bilayer is related to the partitioning of the substance into the apolar part of the fluid bilayer (K_i, eq 2), which is more closely related to the $P_{O/W}$ partition coefficient. From the data in Table 2, we see that even though eosin B readily partitions into the lipid bilayer (high $P_{MO/W}$) it still has a low solubility in the apolar layer of the bilayer (low $P_{O/W}$), which can be explained by the fact that it is charged. A comparison can be made to flip-flop of surfactants embedded in bilayer membranes and the strong rate dependence on their headgroup charge.[54] This means that even though lateral transport, along the bilayer plane, is fast transport across the bilayer is slow, and the eosin B permeability therefore drops considerably when it has to traverse the bilayers in the lamellar part of the membrane.

The experimental data for the effective permeability of metronidazole in a double-porous MO membrane at varying osmotic gradients are shown in Figure 5b. Two things are worth noting in these data. First, the effect of the osmotic gradient on the lipid structure seen in Figure 5a is much less pronounced for metronidazole. Since metronidazole has high solubility in both the aqueous and bilayer regions, the lyotropic lipid phase structure is a minor concern in relation to the diffusional transport, and therefore the permeability does not show as dramatic a decay as for the case of eosin B. However, there does seem to be a decay with increasing osmotic gradient, which can be explained by the fact that the partitioning is not exactly equal to one, and thus the presence of the lamellar phase has a minor influence on the effective permeability. Second, the absolute values of the effective permeability are much higher for metronidazole compared to eosin B. This can be attributed to the smaller size of metronidazole (higher diffusion coefficient) and to the fact that metronidazole partitions more equally between aqueous and lipid domains, thus allowing for a less tortuous path through the lipid phase and access to a larger cross-sectional diffusion area of the membrane, that is, both lipid and water domains.

The effective permeability of 5-HMF across a double-porous MO membrane at varying osmotic gradients is shown in Figure 5c. The data show the same trend as observed for eosin B, although the position of the shift in effective permeability is significantly different between the two cases. This difference can be related to the possibility that the membrane responds not only to the water gradient but also to the gradient in the diffusing substance. This effect can be neglected if the concentration of diffusing drug/dye molecules is low and if the interaction between the drug/dye molecules and the lipid phase is weak. However, this is not the case for 5-HMF, which readily partitions into the MO lipid phase, as is obvious from the partition coefficient $P_{MO/W}$, thus slightly altering the composition of the membrane and possibly also the phase behavior. A bulk sample of MO inside a dialysis membrane placed in a solution containing 5-HMF and PEG 2000 indeed showed a cubic phase at Π_{osm} well above Π_{tr} of pure MO. In other words, 5-HMF indeed shifts the phase transition between the bicontinuous cubic phase to the lamellar phase to higher Π_{osm}, which is also consistent with the results in Figure 5c. Similar behavior has also been shown for other amphiphilic solutes in the MO system.[55] Eosin B is also slightly amphiphilic and partitions into the MO phase. However, we have previously shown that the addition of eosin B has no detectable effect on the phase transitions in the MO system,[10,12] and therefore it is reasonable for that case to perform the analysis only taking into account the response to the osmotic gradient. A final comment on the comparison of the data in Figure 5 is that the quantitative values for the flux are higher for 5-HMF compared to eosin B. This can be explained by the higher partitioning of 5-HMF in the lipid phase compared to the partitioning of eosin B ($P_{MO/W}$(5-HMF) > $P_{MO/W}$(eosin)).

In parallel to the studies of responding MO membranes, we have also briefly looked at transport across double-porous membranes filled with other lipid species, namely, DOPC and *E. coli* total lipid extract. DOPC is expected to form a liquid crystalline lamellar phase at all osmotic pressures investigated,[43] which is also supported by the X-ray data (see section 3.3). If the lamellae are defect-free and aligned perpendicular to the pore direction, P_{eff} should be significantly lower than for MO at all osmotic pressures. However, since the measured P_{eff} is higher than for the MO membranes composed of both lamellar and cubic phase, although lower than the MO cubic phase membrane, we conclude that the DOPC bilayers are only partially oriented or contain defects. For *E. coli* total lipid extract, the X-ray data are not conclusive, and P_{eff} is in the same order of magnitude as for DOPC.

Finally, we performed control experiments to ensure that the stepwise change in membrane permeability observed for eosin B and 5-HMF is due to changes in the lipid membrane and not an artifact in the system. We performed experiments with only a dialysis membrane, without lipid or polymer scaffold membrane. The results showed no abrupt change in permeability, and the only effect observed was related to the dilution of the donor phase solution due to high water flux across the membrane. Similar control experiments for metronidazole flux across silicone membranes[13] and eosin B transport across hydrophilic Polypro membranes[12] in the presence of an osmotic gradient also verify that the observed change in permeability does not occur in these nonresponding membranes. We therefore conclude that the observed response in effective permeability to the variation in osmotic gradient is due to induced changes in the responding lipid membrane.

3.6. Theoretical Modeling of Drug/Dye Transport in Responding Double-Porous Track-Etch MO Membranes. There is a large body of work on the MO equilibrium phase behavior and structure available in the literature.[33,40,41,56−58] Furthermore, water diffusion through the MO *Ia*3*d* cubic phase[59] and lipid bilayers[60] has also been studied. Upon the basis of this experimental data and modeling, we have previously presented a detailed thermodynamical model for diffusive transport through a MO membrane exposed to gradients in both Π_{osm} and a control substance (such as eosin B).[10,12] The main assumptions in this model are that the gradient in Π_{osm} solely determines the structure (i.e., that the control substance has a negligible influence) and that the local structure and phase behavior can be determined from the local Π_{osm}.

In the present study, the double-porous track-etch membrane was placed between two dialysis membranes. While the dialysis membranes are completely permeable to water, they constitute a significant, but unknown, hindrance to diffusion of the control substances (the dye or drug). We assume that the permeability of the dialysis membranes, P_{dialys}, does not depend on the concentration of the control substance, meaning that they do not

constitute responding membranes. To circumvent the problem of the unknown value of P_{dialys}, we will here only discuss the permeability of the system *after* induction of the lamellar phase, as detailed below.

The total permeability, P_{eff}, of the full system for the control substance can be written as[61]

$$\frac{1}{P_{eff}} = \frac{1}{P_{dialys}} + \frac{1}{P_{cubic}} + \frac{1}{P_{lam}} + \frac{1}{P_{aq}} \quad (3)$$

where P_{cubic} is the permeability of the cubic phase, P_{lam} the permeability of the lamellar phase, and P_{aq} the permeability of the aqueous regions within the part of the pores that is not filled by lipid phases. The permeability of the cubic phase and the permeability of the lamellar phase both depend on the osmotic gradient; the permeability of the dialysis membranes does, by assumption, not. Furthermore, as the total thickness of the MO membrane does not change significantly with an increasing osmotic gradient (once the lamellar phase is formed), it is a good approximation to assume that the permeability of the aqueous regions inside the pores does not depend on the osmotic gradient. We can, within the stated approximations, therefore use the previously developed model for the sum $1/P_{cubic} + 1/P_{lam}$ and adjust the remaining (constant) terms such that the experimentally determined permeability when only the cubic phase is present is reproduced. In this way, a description of the induction of the lamellar phase is feasible, despite the unknown permeability of the dialysis membranes.

Figure 5a,b shows the result of the model under these assumptions, obtained with only two free parameters. These are the permeability of the membrane when only the cubic phase is present and the permeability of a bilayer of the lamellar phase to the control substance. The model shows a good description of the experimental data over a large range of osmotic pressure gradients. On the basis of this, we can extract the permeability of a lipid bilayer to eosin B and metronidazole as 150 nm/s and 110 μm/s, respectively. These values are considered reasonable, and the large difference in permeability of these substances is expected on the grounds that eosin B is charged while metronidazole is not. The present model does not hold for the third substance, 5-HMF, as this control substance apparently affects the membrane structure, and the assumptions made in the model are therefore not valid for this case. This would require an extended theoretical description including coupled transport processes,[62] which goes beyond the scope of the present presentation. A basic assumption in the theoretical model is the alignment of the lamellar phase with the bilayer normal parallel to the direction of transport. The good agreement between the experimental data and model therefore suggests that an appropriate alignment of the lamellar phase has been achieved.

3.7. Thermally Induced Phase Transitions in Confinement. The confinement of the lyotropic lipid phase inside the cylindrical pores did not significantly alter the structure of the lyotropic phase, as confirmed by the SAXS measurements. Still, it is possible that the confinement inside small cylindrical pores can give rise to capillary induced phenomena,[15,39] which would affect the phase transitions. This would then depend on both the surface properties of the polymer scaffold membrane, which govern the interaction with the different lipid phases (and the solvent), as well as the radius and surface area of the cylindrical pores.[15]

For the MO system we investigated the transition induced by changes in Π_{osm}, using two different drugs/dyes sensitive to lipid phase structure, as described above (section 3.5). With eosin B,

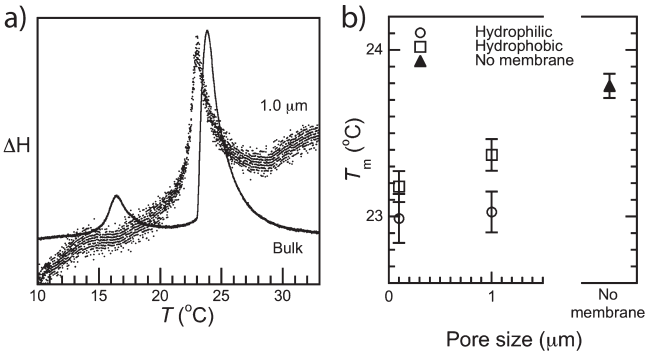

Figure 6. (a) DSC graph of hydrated, DMPC-filled 1.0 μm hydrophobic membranes and bulk DMPC, respectively. Note that the two samples are plotted on a different *y*-axis, to allow easy comparison. (b) Summary of main melting transitions (mean ± SEM) for hydrated DMPC in membrane pores and in bulk.

the phase transition took place at the expected Π_{osm}, but with 5-HMF a cubic structure was retained at much higher Π_{osm}. The apparent shift in the phase transition is explained by that the diffusing drug/dye also influences the phase behavior of the lyotropic phases, shifting the phase boundaries. In these studies, additional effects on the phase transition due to the confinement cannot be ruled out. To assess this question, we performed studies of lipid phase transitions in double-porous membranes in the absence of drug/dye. This was done in a set of experiments using DSC. A major difficulty in these studies that was also recognized for the SAXS measurements described above is the low amounts of lipid sample incorporated inside the pores of the scaffold. Thus, the effective amount of lipid in the samples was 0.05−0.1 mg, which is very close to the detection limit, as is obvious from the signal-to-noise ratio in Figure 6a. To enable measurements of transition temperatures of lipids inside the pores, we chose a system with high-enthalpy transition (chain melting), rather than the low-enthalpy bicontinuous cubic-lamellar phase transition. For these studies, we used fully hydrated DMPC confined in polymer scaffold membranes with different surface properties (hydrophilic and slightly hydrophobic) and different pore diameters (0.1 and 1.0 μm). Fully hydrated bulk DMPC samples in pure water exhibited two endothermic transitions on heating, a lower temperature, lower enthalpy pretransition (T_{pr}) at 16.0 ± 0.08 °C (mean ± SEM), and a higher temperature, higher enthalpy main transition (T_m) at 23.8 ± 0.07 °C. The measured transition temperature and transition enthalpies (see Figure 6b), are in good agreement with literature data.[63] The pretransition is not always visible in the cooling direction, which is likely due to kinetic delays involving metastable states.[64]

When the hydrated DMPC is confined inside pores with diameter of 1.0 or 0.1 μm, the lipid pretransition cannot be detected, and the T_m is slightly lower compared to T_m measured in bulk, as illustrated in Figure 6. Similar observations were done for hydrophobic and slightly hydrophilic polymer scaffold membranes. When comparing the different systems, we note that the lowest T_m was detected for the smaller pores and for the hydrophilic membranes. The same effect on main transition temperature was seen in the cooling as in the heating direction.

The lower main transition temperature in hydrophilic scaffold membranes compared to hydrophobic ones indicates that the L_α phase is slightly more stable relative to the L_β phase in the hydrophilic scaffold. The larger effect with the smaller pore diameter

also seems reasonable, as any capillary effects induced should be more pronounced in the smaller pores. In contrast to our data, DMPC confined in 0.2 μm AAO membranes showed slightly higher transition temperatures compared to bulk samples,[29] but as pointed out earlier the AAO membranes are rather hydrophilic, thereby having quite different lipid−surface interactions.

The simplest explanation for the disappearance of the pretransition of DMPC upon confinement into pores would be that the rippled phase is destabilized due to the confinement. Indeed, the formation of the rippled P_β gel phase is very sensitive to the conditions and is generally destabilized in unilamellar vesicles[65] and in solid supported bilayers[66] and upon small additions of, for example, urea,[67] cholesterol,[68] gramicidin,[69] or cyclosporine.[70] In contrast, studies on DMPC confined inside porous AAO (pore diameter ∼0.2 μm on one side, 0.02 μm on the opposite) displayed the pretransition.[29] In that case, lipid vesicles were either deposited on the substrate, leaving a multilayer of up to four bilayers, or pushed repeatedly back and forth through the AAO membrane using a liposome extruder and then flushed with water, leaving only a single lipid bilayer covering the pore walls. In other words, in neither of these cases were the pores completely filled with lipid, as in our system. Finally, it cannot be completely ruled out that the pretransition might still be present, though too small to be detected.

4. CONCLUSIONS

Different lipids, MO, DOPC, DMPC, and *E. coli* total lipid extract, have been successfully confined inside the cylindrical pores of well-defined polycarbonate scaffold membranes, as verified by confocal laser scanning microscopy. Though the amount of lipid inside the scaffold membrane is very low, the structure of the lipid inside the membrane pores could successfully be characterized using synchrotron SAXS. The lipid phase structure inside the pores of the scaffold membrane showed no significant difference in phase behavior compared to bulk lipid samples. DSC measurements on hydrated DMPC showed a small decrease in the main transition temperature and a disappearance of the pretransition, when the lipid was confined inside the porous membrane. The effects were most pronounced for the smaller (0.1 μm) diameter pores and hydrophilic membranes.

The double-porous membrane systems were explored in studies of diffusional transport of model substances in the presence of an external osmotic gradient. For a MO membrane, the osmotic gradient can induce a phase change at some position inside the membrane, thus affecting the membrane permeability to polar and apolar substances. We show that the transition from a bicontinuous cubic phase to a lamellar phase in parts of the membrane can lead to a 100-fold decrease in membrane permeability, thus demonstrating how this osmotic gradient can be used as a switch to regulate the membrane barrier. The magnitude of this effect depends on the properties of the diffusing substance. For the special case when the substance partitions equally between the bilayer and water, the permeability was shown to be almost independent of the osmotic gradient. Finally, the experimental transport data show very good agreement with the solute transport predicted from theoretical modeling assuming bilayers oriented with the normal parallel to the pore wall.

■ ASSOCIATED CONTENT

Supporting Information. More detailed discussion of the theoretical model applied to transport through track-etch membranes and its numerical evaluation. This material is available free of charge via the Internet at http://pubs.acs.org.

■ AUTHOR INFORMATION

Corresponding Author

*Correspondence should be addressed to current affiliation: Faculty of Health and Society, Malmö University, SE-205 06 Malmö, Sweden. E-mail: peter.r.nilsson@mah.se. Phone: +46(0)406657881. Fax: +46(0)406658100. Has prior publications under the name Peter Nilsson.

Present Addresses

[§]Department of Applied Physics, Chalmers University of Technology, SE-412 96 Göteborg, Sweden.

■ ACKNOWLEDGMENT

The authors kindly acknowledge Marie Wahlgren, department of Food Technology, Lund University, for access to the DSC equipment; Bo Holmqvist and Peter Ekström, ImaGene-iT, Lund, Sweden, for technical and scientific imaging support during establishment of the confocal microscopy analysis; MAX-lab, Lund University, Sweden, for allocation of beam time; Yngve Cerenius, Dörthe Haase, and Tomás Plivelic for help with the SAXS experiments; Tommy Nylander, Physical Chemistry, Lund University and Göran Lindblom, Umeå University for fruitful discussions. Financial support by the Swedish Research Council (VR) through the Linnaeus Center of Excellence on Organizing Molecular Matter (OMM) is gratefully acknowledged. The Swedish Foundation for Strategic Research (ES) and the Swedish Research Council (ES) are also acknowledged for financial support.

■ REFERENCES

(1) Elias, P. M. *J. Invest. Dermatol.* **1983**, *80*, 44–9.
(2) Davis, A. D.; Weatherby, T. M.; Hartline, D. K.; Lenz, P. H. *Nature* **1999**, *398*, 571–571.
(3) Dratz, E. A.; Hargrave, P. A. *Trends Biochem. Sci.* **1983**, *8*, 128–131.
(4) Williams, M. C. *J. Cell Biol.* **1977**, *72*, 260–277.
(5) Almsherqi, Z. A.; Landh, T.; Kohlwein, S. D.; Deng, Y. *Int. Rev. Cell Mol. Biol.* **2009**, *274*, 275–342.
(6) Lindblom, G.; Rilfors, L. *Biochim. Biophys. Acta, Rev. Biomembr.* **1989**, *988*, 221–56.
(7) Larsson, K. *Curr. Opin. Colloid Interface Sci.* **2000**, *5*, 64–69.
(8) Shearman, G. C.; Ces, O.; Templer, R. H.; Seddon, J. M. *J. Phys.: Condens. Matter* **2006**, *18*, S1105–S1124.
(9) Norlen, L. *J. Invest. Dermatol.* **2001**, *117*, 823–829.
(10) Åberg, C.; Pairin, C.; Costa-Balogh, F. O.; Sparr, E. *Biochim. Biophys. Acta, Biomembr.* **2008**, *1778*, 549–558.
(11) Sparr, E.; Wennerström, H. *Biophys. J.* **2001**, *81*, 1014–1028.
(12) Costa-Balogh, F. O.; Åberg, C.; Sousa, J. J. S.; Sparr, E. *Langmuir* **2005**, *21*, 10307–10310.
(13) Björklund, S.; Engblom, J.; Thuresson, K.; Sparr, E. *J. Controlled Release* **2010**, *143*, 191–200.
(14) Hadgraft, J.; Lane, M. E. *Int. J. Pharm. Tech. Prod.* **2005**, *305*, 2–12.
(15) Evans, D.; Wennerström, H. *The colloidal domain: where physics, chemistry, biology, and technology meet*, 2nd ed.; Wiley-VCH: New York, 1999.

(16) von Klitzing, R.; Thormann, E.; Nylander, T.; Langevin, D.; Stubenrauch, C. *Adv. Colloid Interface Sci.* **2010**, *155*, 19–31.
(17) Elias, P. M. *J. Controlled Release* **1991**, *15*, 199–208.
(18) Charalambopoulou, G. C.; Steriotis, T. A.; Mitropoulos, A. C.; Stefanopoulos, K. L.; Kanellopoulos, N. K.; Ioffe, A. *J. Invest. Dermatol.* **1998**, *110*, 988–90.
(19) Gitsas, A.; Floudas, G.; Butt, H. J.; Pakula, T.; Matyjaszewski, K. *Macromolecules* **2010**, *43*, 2453–2462.
(20) Wu, Y.; Cheng, G.; Katsov, K.; Sides, S. W.; Wang, J.; Tang, J.; Fredrickson, G. H.; Moskovits, M.; Stucky, G. D. *Nat. Mater.* **2004**, *3*, 816–822.
(21) Kim, E.-M.; Jung, J.-S.; Chae, W.-S. *Chem. Commun. (Cambridge, U.K.)* **2010**, *46*, 1760–1762.
(22) Apel, P. *Radiat. Meas.* **2001**, *34*, 559–566.
(23) Groen, D.; Gooris, G. S.; Ponec, M.; Bouwstra, J. A. *Biochim. Biophys. Acta, Biomembr.* **2008**, *1778*, 2421–2429.
(24) Idziak, S. H. J.; Koltover, I.; Davidson, P.; Ruths, M.; Li, Y.; Israelachvili, J. N.; Safinya, C. R. *Phys. B (Amsterdam, Neth.)* **1996**, *221*, 289–295.
(25) Tabaei, S. R.; Jönsson, P.; Bränden, M.; Höök, F. *J. Struct. Biol.* **2009**, *168*, 200–206.
(26) Mueller, P.; Rudin, D. O. *Nature* **1967**, *213*, 603–4.
(27) Mey, I.; Stephan, M.; Schmitt, E. K.; Muller, M. M.; Ben Amar, M.; Steinem, C.; Janshoff, A. *J. Am. Chem. Soc.* **2009**, *131*, 7031–7039.
(28) Nikolelis, D. P.; Siontorou, C. G. *Anal. Chem.* **1995**, *67*, 936–44.
(29) Alaouie, A. M.; Smirnov, A. I. *Langmuir* **2006**, *22*, 5563–5565.
(30) Guegan, R.; Morineau, D.; Lefort, R.; Beziel, W.; Guendouz, M.; Noirez, L.; Henschel, A.; Huber, P. *Eur. Phys. J. E* **2008**, *26*, 261–273.
(31) Landh, T. *J. Phys. Chem.* **1994**, *98*, 8453–67.
(32) Hyde, S. T. *Langmuir* **1997**, *13*, 842–851.
(33) Qiu, H.; Caffrey, M. *Biomaterials* **2000**, *21*, 223–34.
(34) Knaapila, M.; Svensson, C.; Barauskas, J.; Zackrisson, M.; Nielsen, S. S.; Toft, K. N.; Vestergaard, B.; Arleth, L.; Olsson, U.; Pedersen, J. S.; Cerenius, Y. *J. Synchrotron Radiat.* **2009**, *16*, 498–504.
(35) Cerenius, Y.; Ståhl, K.; Svensson, L. A.; Ursby, T.; Oskarsson, Å.; Albertsson, J.; Liljas, A. *J. Synchrotron Radiat.* **2000**, *7*, 203–8.
(36) Stanley, C. B.; Strey, H. H. *Macromolecules* **2003**, *36*, 6888–6893.
(37) Gonzalez-Tello, P.; Camacho, F.; Blazquez, G. *J. Chem. Eng. Data* **1994**, *39*, 611–14.
(38) Parsegian, V. A.; Rand, R. P.; Fuller, N. L.; Rau, D. C. *Methods Enzymol.* **1986**, *127*, 400–16.
(39) Wennerström, H.; Thuresson, K.; Linse, P.; Freyssingeas, E. *Langmuir* **1998**, *14*, 5664–5666.
(40) Chung, H.; Caffrey, M. *Nature* **1994**, *368*, 224–6.
(41) Sparr, E.; Wadsten, P.; Kocherbitov, V.; Engström, S. *Biochim. Biophys. Acta, Biomembr.* **2004**, *1665*, 156–166.
(42) Ridell, A. Thesis, *Uppsala University*, 2003.
(43) Parsegian, V. A.; Fuller, N.; Rand, R. P. *Proc. Natl. Acad. Sci. U.S.A.* **1979**, *76*, 2750–4.
(44) Staudegger, E.; Prenner, E. J.; Kriechbaum, M.; Degovics, G.; Lewis, R. N. A. H.; McElhaney, R. N.; Lohner, K. *Biochim. Biophys. Acta, Biomembr.* **2000**, *1468*, 213–230.
(45) Morein, S.; Andersson, A.; Rilfors, L.; Lindblom, G. *J. Biol. Chem.* **1996**, *271*, 6801–9.
(46) Römer, W.; Steinem, C. *Biophys. J.* **2004**, *86*, 955–965.
(47) Nieh, M. P.; Raghunathan, V. A.; Wang, H.; Katsaras, J. *Langmuir* **2003**, *19*, 6936–6941.
(48) Sparr, E.; Wennerström, H. *Colloids Surf., B* **2000**, *19*, 103–116.
(49) Marrink, S. J.; Berendsen, H. J. C. *J. Phys. Chem.* **1996**, *100*, 16729–16738.
(50) Nagle, J. F.; Mathai, J. C.; Zeidel, M. L.; Tristram-Nagle, S. *J. Gen. Physiol.* **2008**, *131*, 77–85.
(51) Kasprzyk-Hordern, B.; Dinsdale, R. M.; Guwy, A. J. *J. Chromatogr., A* **2007**, *1161*, 132–145.
(52) Loke, M.-L.; Tjornelund, J.; Halling-Sorensen, B. *Chemosphere* **2002**, *48*, 351–361.
(53) Engström, S.; Norde, T. P.; Nyquist, H. *Eur. J. Pharm. Sci.* **1999**, *8*, 243–254.
(54) Yaroslavov, A. A.; Udalykh, O. Y.; Melik-Nubarov, N. S.; Kabanov, V. A.; Ermakov, Y. A.; Azov, V. A.; Menger, F. M. *Chem.—Eur. J.* **2001**, *7*, 4835–4843.
(55) Engström, S.; Engström, L. *Int. J. Pharm.* **1992**, *79*, 113–22.
(56) Turner, D. C.; Wang, Z. G.; Gruner, S. M.; Mannock, D. A.; McElhaney, R. N. *J. Phys. II* **1992**, *2*, 2039–63.
(57) Nollert, P.; Qiu, H.; Caffrey, M.; Rosenbusch, J. P.; Landau, E. M. *FEBS Lett.* **2001**, *504*, 179–186.
(58) Anderson, D. M.; Gruner, S. M.; Leibler, S. *Proc. Natl. Acad. Sci. U.S.A.* **1988**, *85*, 5364–8.
(59) Feiweier, T.; Geil, B.; Pospiech, E.-M.; Fujara, F.; Winter, R. *Phys. Rev. E: Stat., Phys., Plasmas, Fluids, Relat. Interdiscip. Top.* **2000**, *62*, 8182–8194.
(60) Graziani, Y.; Livne, A. *J. Membr. Biol.* **1972**, *7*, 275–84.
(61) Crank, J. *The Mathematics of Diffusion*; Oxford University Press: Oxford, 1975.
(62) Åberg, C.; Wennerström, H. *Phys. Chem. Chem. Phys.* **2009**, *11*, 9075–9081.
(63) Janiak, M. J.; Small, D. M.; Shipley, G. G. *J. Biol. Chem.* **1979**, *254*, 6068–78.
(64) Cho, K. C.; Choy, C. L.; Young, K. *Biochim. Biophys. Acta, Lipids Lipid Metab.* **1981**, *663*, 14–21.
(65) Heerklotz, H.; Seelig, J. *Biophys. J.* **2002**, *82*, 1445–1452.
(66) Johnson, S. J.; Bayerl, T. M.; McDermott, D. C.; Adam, G. W.; Rennie, A. R.; Thomas, R. K.; Sackmann, E. *Biophys. J.* **1991**, *59*, 289–94.
(67) Costa-Balogh, F. O.; Wennerström, H.; Wadsö, L.; Sparr, E. *J. Phys. Chem. B* **2006**, *110*, 23845–23852.
(68) Malcolmson, R. J.; Higinbotham, J.; Beswick, P. H.; Privat, P. O.; Saunier, L. *J. Membr. Sci.* **1997**, *123*, 243–253.
(69) Prenner, E. J.; Lewis, R. N.; Kondejewski, L. H.; Hodges, R. S.; McElhaney, R. N. *Biochim. Biophys. Acta* **1999**, *1417*, 211–23.
(70) Lambros, M. P.; Rahman, Y. E. *Chem. Phys. Lipids* **2004**, *131*, 63–69.
(71) *SciFinder*, Calculated using Advanced Chemistry Development (ACD/Labs) Software V8.14 for Solaris (1994—2010 ACD/Labs), 2010.
(72) Merck Chemicals (Germany), Product data eosin B.